Analysis of a continuous-time adaptive voter model

Emmanuel Kravitzch, Yezekael Hayel, Vineeth Varma, Antoine O Berthet

Analysis of a Continuous-Time Adaptive Voter Model

Emmanuel Kravitzch and Yezekael Hayel*
Laboratoire Informatique d'Avignon (LIA), Avignon Université†

Vineeth S. Varma‡
Université de Lorraine, CNRS, CRAN, F-54000 Nancy, France. §

Antoine O. Berthet
Laboratoire des Signaux et Systèmes (L2S), Université Paris-Saclay, CNRS, CentraleSupélec. ¶

(Dated: December 14, 2022)

Abstract– In this paper, we study a novel variant of the voter model on adaptive networks in which nodes can flip their spin, create new connections or break existing connections. We first perform an analysis based on the mean-field approximation to compute asymptotic values for macroscopic estimates of the system, namely the total mass of present edges in the system and the average spin. However, numerical results show that this approximation is not very suitable for such a system, for which it does not capture key features such as the network breaking into two disjoint and opposing (in spin) communities. Therefore, we propose another approximation based on an alternate coordinate system to improve accuracy and validate this model through simulations. Finally, we state a conjecture dealing with the qualitative properties of the system, corroborated by numerous numerical simulations.

Keywords– Voter models, adaptive voter models, spin systems, complex social networks.

I. INTRODUCTION

A. Research context and literature review

In the last decades, models of statistical mechanics have been extensively studied to describe a wide spectrum of complex phenomena, ranging from ferromagnetism to biochemical interactions. Social systems and collective phenomena are also under the scope of the aforementioned framework. In this case, the particles are agents that influence each other according to simple rules. One of the main models is a spin system called the voter model (VM) first introduced by Thomas Liggett [1] and defined as follows. Consider a population of agents of size K and index by an integer k each agent, $k \in [\![1, K]\!]$. At all times $t \geq 0$, each agent k is endowed with a binary value $X_k(t) \in \{+1, -1\}$. These two values represent two opposite orientations that may be opinions, consumer preferences, behaviors, etc. Across time, the agents may change their spin under the influence of others, leading to a *stochastic process*. Since Liggett's seminal work, the VM has attracted a lot of attention and numerous refinements have been explored, e.g., nonlinear voter models [2], with stubborn agents [3] or contrarian [4], including noise [5]. A comprehensive survey can be found in[6].
By the way, the word *voter* should be taken in a very abstract sense: it may actually model any situation where some agents have to make a repeated choice between several possibilities, here two for sake of simplicity. Specifically, in the context of social networks, the main mechanisms shaping the social dynamics are *social mimetism*, *homophily* and *selective exposure*. Social mimetism is the behaving trend involving synchronization of one's own opinions with those of the imitated person. Homophily is the trend one has to connect with alike people, alike simply means having the same spin in the VM formalism. Analogously, selective exposure is the trend one has to dismiss dissonant neighbors, that is agents having an opposite spin. These notions have been thoroughly described by psychosocial studies [7, 8] and then taken for granted in this work. While VMs over *static* graphs encompass social mimetism, they fail to encompass selective exposure and homophily. In order to keep track of these last two key characteristics, we have to consider a model where the graph is *adaptive*, evolving according to the spin profile $\big(X_k\big)_{k\in[\![1,K]\!]}$. Models of this kind are said *coevolutionary* [9] or *adaptive* and are the focus of this work. Though more recent and less studied than systems over static graphs, adaptive voter models (AVMs) are the subject of growing interest, e.g., in the context of epidemics [10]. By allowing the edges to evolve, a wide choice of network dynamics is worth considering. Some authors define a local linkage mechanism [11, 12], called *triadic closure* or *transitivity reinforcement*, where agents only seek new friends among their 2-hop neighbors. Nevertheless, the main model is the one proposed in [13] with two possible opinions. It is an AVM with a simple linking rule: when agent l breaks his tie with agent m, he immediately reconnects to another agent p, the latter being uniformly chosen over the whole population (*rewire-to-random)*. See for instance [14, 15] and references therein.

* https://sites.google.com/site/yezekaelhayelsite/
† emmanuel.kravitzch@alumni.univ-avignon.fr
‡ https://sites.google.com/site/vineethshome/
§ vineeth.satheeskumar-varma@univ-lorraine.fr
¶ antoine.berthet@centralesupelec.fr

Sometimes, rewiring is done only among like-minded people, that is people of the same spin (*rewire-to-same*). The main difference in the model studied here is that breaking and linking are done simultaneously, hence the total mass of edges is conserved. The refinement we propose is to allow edge breaks and edge creations separately. In this model, the degree distribution is then dynamic, increasing the range of possible configurations. In particular, the degree distribution can evolve.

B. Motivation and main contributions

Among the traditional questions raised by such statistical mechanics models, the most classical one is that of the *phase transition*. It is well known that in VMs, several radically different regimes can be observed depending on the model's parameters: in the case of static graphs, the two types of spins can survive - this case is mentioned as *coexistence* in [1], also called *metastable* regime; or on the contrary one spin can rapidly conquer all the agents: in this case, we talk about *consensus*. After reaching consensus, the dynamics stops, consensus is said to be an *absorbing* configuration. When defining model's parameters, there are range of values dedicated to each of the phase, and there exists (surface of) values at the boundary, whence the term *phase transition*. In the case of adaptive networks, the situation is a bit different. One may have clustering according to the spins. Thus, both spins are preserved but the two clusters are completely separated. On the contrary, a third possibility is the coexistence of disagreeing agents among same connected components. In this case, some links between the two community of spins, named *discordant* links and properly defined in the sequel, maintains. Hence, global consensus is simply a very particular case of the first scenario.

In this paper, instead of tracking threshold values for phase transitions, as it has been done in [16], we rather strive to give qualitative results about the macroscopic behaviour of the coupled dynamics. The main contributions are the following:

- In the dense graph regime, we highlight the homogeneous behaviour and the existence of a continuous trajectory which might be the limiting system as $K \to +\infty$. It is notable that this phenomenon is independent of the model's parameters. Further investigations may uncover the very nature of this object.
- We also provide quantitative results: by a change of coordinates, we identify the surface of equilibria, and estimate the limiting discordance (namely the mass of discordant edges) for the metastable regime. This estimation shows very good results compared to the standard mean-field approximation applied to the natural edges-spins coordinates.
- Finally, a linearization based analysis of the reduced-order system around the points corresponding to absorbing states, provides a reasonable approximation of the phase transition that occurs in the initial stochastic system.

In the remainder of the paper, Section II presents the model. Section III analyzes the model using the standard mean-field approximation. Section IV refines the analysis by introducing a change of coordinates partitioning the edges into blocks. Section V formulates a conjecture and supports it with numerous numerical simulations. Section VI concludes the article and indicates avenues for future research. The table below summarizes some notations.

Object definition	Formula	Symbol
population index	$\{1, ..., K\}$	$[K]$
unweighted digraph	$a_{lm} = 0$ or 1	A
complete graph	$\mathbb{K}_{lm} = 1 \forall l, m \in [K]$	$\mathbb{K}$
Hadamard product	$(A \odot B)_{ij} = a_{ij} b_{ij}$	$\odot$
i^{th} unitary vector of $\mathbb{R}^K$		e_i
0 matrix with 1 at only lm	$e_l e_m^T$	e_{lm}
all-1 vector	$\sum_j e_j$	$\mathbb{1}$
indicator U	1 if U occurs, 0 else	$\mathbb{1}_U$

II. MODEL

Let us define a population of agents of size $K \geq 1$ evolving and interacting over time. At all time $t \geq 0$, each agent $k \in \{1, ..., K\}$ (denoted by $[K]$ for short) is endowed with a binary value $X_k(t) = \pm 1$ called a *spin*. The spin can represent an orientation, a preference or any other individual state. The term "spin" comes from the analogy with magnetization models, and is already used in early works on voter models over lattices. We then keep it throughout the text by commodity. The vector $X(t) := \big(X_k(t)\big)_{k \in [K]} \in \{+1, -1\}^K$ is the *spin profile* at time t. The agents interact through a dynamic graph $\mathcal{G}_t$, the latter *co-evolving* with the spin profile. Throughout this work, the graph $\mathcal{G}_t$, supposed to be unweighted and directed, is represented by its adjacency matrix $A(t) \in \{0, 1\}^{K^2}$. We have that $a_{lm}(t) = 1$ if and only if there is a link from agent l to agent m at time t. In the sequel, we also use the generalized notation: for two subsets $U, V \subset [K]$ we denote by $a_{UV} := \sum_{l \in U, m \in V} a_{lm}$.

The overall process (X^K, A^K) (the dependence in K will be omitted when it is clear from the context) then evolves in the finite state space $\mathcal{S}_K := \{+1, -1\}^K \times \{0, 1\}^{K^2}$. The rates associated to the coevolution dynamics, namely the nodes' dynamics and the edges 'one

are now introduced. The dynamics of agents' spins correspond to the standard linear VM, already abundantly analysed over regular lattices (chapter V of [1] and part II of [17]) and more recently over heterogeneous and random graphs [18, 19]. It models the mimetic behaviour of individuals. Typically, an agent with positive spin (value $+1$) surrounded by agents displaying negative spin (value -1) is very likely to flip because of the influence of the neighbours. The flip rate of agent $k \in [K]$ is given by:

$$\text{flip: } (X, A) \longrightarrow (X - 2X_k e_k, A) \text{ at rate}$$
$$\Phi(k; X, A) = \phi \sum_{j \in [K]} A_{kj} \mathbb{1}_{(X_k \neq X_j)} \quad (1)$$

where e_k is the k^{th} unit vector of $\mathbb{R}^K$. The voter step is said to be linear because the rate to flip is linear with respect to the number of disagreeing neighbors. In this regard, the parameter $\phi > 0$ can be interpreted as the persuadability coefficient, equal for all agents.

On top of this linear flip dynamics, we consider the following edges' dynamics. It takes into account two important properties that are characteristic of social interactions, namely *homophily* and *selective exposure*. As mentioned in the introduction, they respectively correspond to the trend one has to create links with alike people on one hand and to dismiss disagreeing neighbors on the other hand. These two features have been copiously described by psycho-social studies [7, 20] and are nowadays well recognized to play a structural role in social dynamics. Then, for any individuals $l, m \in [K]$, the rate for link creation and link deletion (when it exists) are respectively defined as follows:

$$\text{link creation: } (X, A) \longrightarrow (X, A + e_{lm}) \text{ at rate}$$
$$\Gamma(lm; x, A) = \gamma(1 - A_{lm}) \underbrace{\mathbb{1}_{(X_l = X_m)}}_{\text{homophily}} \quad (2)$$

where one shall remember that we are dealing with a *directed* graph and $e_{lm} = e_l e_m^T$ is the unitary matrix with a 1 at entry (l, m) and only 0's everywhere else, and

$$\text{link deletion: } (X, A) \longrightarrow (X, A - e_{lm}) \text{ at rate}$$
$$B(lm; x, A) = \beta A_{lm} \underbrace{\mathbb{1}_{(X_l \neq X_m)}}_{\text{selec. exposure}} \quad (3)$$

where γ (resp. β) is the propensity of one agent l to get connected (resp. disconnected) to another agent m endowed with the same spin (resp. with opposite spin).

For any $f : \mathcal{S}_K \mapsto \mathbb{R}$, the associated generator $Q : \mathbb{R}^{\mathcal{S}_K} \mapsto \mathbb{R}^{\mathcal{S}_K}$ allows to characterize the Markov process by a single formula. Then,

$$\begin{aligned}(Qf)(x, a) = &\sum_k \Phi(k; x, a) \left[f(x - 2e_k x_k, a) - f(x, a)\right] \\ &+ \sum_{lm} \Gamma(lm; x, a) \left[f(x, A + e_{lm}) - f(x, a)\right] \\ &+ \sum lmB(lm, x, A) \left[f(x, a - e_{lm}), f(x, a)\right]. \end{aligned} \quad (4)$$

Note that if the rate parameters ϕ, γ, and β are in the same range, the agents' spin dynamics (1) is, therefore, K times faster compared to the edge stones given by (2) and (3). Since we are interested in the coevolution of the two dynamics (spin and graph) at the *same time scale*, from now on we consider that the flip rate is in the same range as the others and thus $\phi = O(\gamma/K)$.

The Markov process (X^K, A^K) can equivalently be described by a set of *stochastic differential equations* (SDEs) driven by $3K^2$ independent Poisson point processes $\mathcal{N}_{kj}^{\alpha}$ of intensity α with $(k, j) \in [K]^2$ and $\alpha \in \{\frac{\phi}{K}, \beta, \gamma\}$:

$$\begin{cases} dX_k(t) = -2X_k(t^-) \sum_j A_{kj}(t^-) \mathbb{1}_{(X_k(t^-) \neq X_j(t^-))} \mathcal{N}_{kj}^{\phi/K}(dt) \\ dA_{lm}(t) = (1 - A_{lm}(t^-)) \mathbb{1}_{(X_l(t^-) = X_m(t^-))} \mathcal{N}_{lm}^{\gamma}(dt) \\ \qquad\qquad - A_{lm}(t^-) \mathbb{1}_{(X_l(t^-) \neq X_m(t^-))} \mathcal{N}_{lm}^{\beta}(dt) \end{cases} \quad (5)$$

A. Absorbing configurations

When K is finite, it is clear that the VM over static (and adaptive) graphs possesses absorbing configurations (sometimes called *frozen states*), which can be identifiable. In our setting, the Markov process (X^K, A^K) indeed admits the following absorbing states:

$$\mathcal{A} = \Big\{(x, a) \in \mathcal{S}_K : \forall (l, m),\ (x_l = x_m \text{ and } a_{lm} = 1) \quad (6)$$
$$\text{or } (x_l \neq x_m \text{ and } a_{lm} = 0)\Big\}. \quad (7)$$

In words, an absorbing state is then a configuration where the population of individuals is clustered in two separated complete subgraphs denoted by C^+ and C^- with $C^+ \bigcup C^- = [K], C^+ \bigcap C^- = \emptyset$, with $x_l = +1\ \forall l \in C^+$ and $x_k = -1\ \forall k \in C^-$, and with no links between the two blocks: $a_{ij} = a_{ji} = 0\ \forall i \in C^+, \forall j \in C^-$. Furthermore the absorbing configurations are strongly attractive: with probability one, the process gets trapped into one of them after a (random) finite time T_{abs} defined as:

$$T_{abs} := \inf \Big\{t : (X(t), A(t)) \in \mathcal{A}\Big\} < \infty \quad (8)$$

B. Filter bubbles and discordance

When the stochastic process (X, A) has reached an absorbing state, then it stops: each agent X_k has ultimately chosen his spin and has broken all of his links with the opposite individuals. This configuration represents the emergence of the so-called *filter bubbles*: each one confines himself to a group of people sharing the same opinion, and then has no access to other viewpoints, whence the term *filter bubble*. This phenomenon is suspected to increase radicalization and fake news propagation [21–23]. Detecting and forecasting the emergence of these

bubbles is a major issue in social network analysis. A simple estimator to quantify the filter bubble effect is the *discordance* (sometimes called interface density [5]). This value measures how strongly two opposite communities influence one other. An edge lm is said to be *discordant* if $a_{lm}\mathbb{1}_{(x_l \neq x_m)} = 1$, meaning that a link between individuals l and m exists and the two individuals have opposite spin.

Definition 1 (total discordance)**.** *The total discordance* $\mathcal{D}(x,a)$ *of any configuration* $(x,a) \in \mathcal{S}_K$ *is defined as:*

$$\mathcal{D}(x,a) := \frac{1}{K^2}\sum_{lm} a_{lm}\mathbb{1}_{(x_l \neq x_m)}. \tag{9}$$

If $\mathcal{D}(x,a) = 0$, then it means that (x,a) is close to an absorbing configuration: the node dynamics has stopped, and after the link creation between agreeing agents, the overall process (X,A) will get frozen. Let define the associated hitting time $T_{abs} := \inf\{t > 0 : \mathcal{D}(X(t),A(t)) = 0\}$. The following property, called *slow extinction* [24], properly formalizes metastability.

Definition 2 (slow extinction)**.** *The total discordance slowly extincts if*

$$\exists c > 0, \quad \mathbb{P}\left(T_{abs} < e^{cK}\right) < e^{-cK}. \tag{10}$$

Figure 1 illustrates this phenomenon: we have plotted the extinction time evolution in terms of time to extinction for two different regimes: the sub-critical regime ($\phi \approx \beta$, in blue), and the metastable regime ($\phi \gg \beta$, in red). It is clear that extinction time grows much faster for the metastable regime compared to sub-critical regime. The next section is devoted to a first line of analysis, namely one of the standard mean-field approximation.

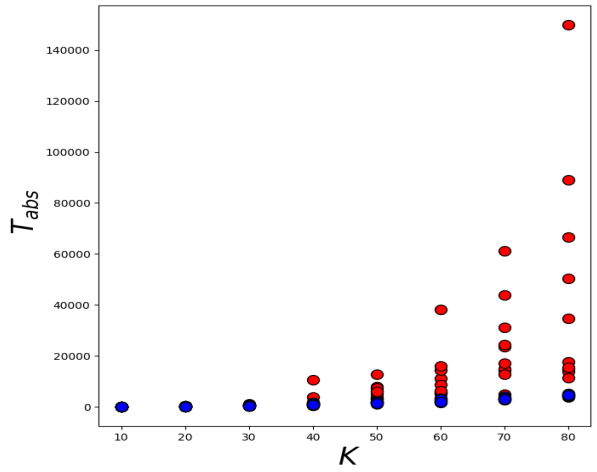

FIG. 1. Extinction time of the process for different number of agents $K = 10, 20, ..., 80$. In each case, 10 simulations have been performed for each regime: in blue, the sub-critical regime: $(\phi,\beta,\gamma) = (1,1,1)$; in red, the metastable one: $(\phi,\beta,\gamma) = (4,1,4)$. *One can see that the absorbing time* T_{abs} *grows much faster in the metastable regime than in the subcritical regime.*

III. A FIRST APPROXIMATION: THE CLASSICAL NIMFA

The principle of the N-intertwined mean-field approximation (NIMFA) [25] is to consider that when the number of particles in the system is high, independence between particles state emerges, and then we have $\mathbb{E}X_kX_j = \mathbb{E}X_k\mathbb{E}X_j$. Thus applying this approximation by considering large number of agents, we can assume that $\mathbb{E}A_{lm}(t)X_k(t) = \mathbb{E}A_{lm}(t)\mathbb{E}X_k(t)$. Introducing the variables $x(t) := \mathbb{E}X(t) \in [-1,1]^K$, $a(t) := \mathbb{E}A(t) \in [0,1]^{K^2}$, taking both lines of (5) under expectation $\mathbb{E}[.]$, and assuming independence between particles yields the associated NIMFA system for (x,a):

$$\begin{cases} \dot{x}_k &= \frac{\phi}{K}\sum_j a_{kj}(x_j - x_k) \\ \dot{a}_{lm} &= \gamma(1-a_{lm})\underbrace{\frac{1+x_lx_m}{2}}_{homophily} - \beta a_{lm}\underbrace{\frac{1-x_lx_m}{2}}_{sel.\ exp.} \end{cases} \tag{11}$$

In matrix form, it reads

$$\begin{cases} \dot{x} &= \frac{\phi}{K}\left(A - diag(A\mathbb{1})\right)x \\ \dot{a} &= \gamma\left(\mathbb{K} - a\right) \odot \frac{\mathbb{K}+xx^T}{2} - \beta a \odot \frac{\mathbb{K}-xx^T}{2} \end{cases} \tag{12}$$

where $diag(u)$ is the diagonal matrix $\Big(diag(u)\Big)_{lm} := u_l\mathbb{1}_{(l=m)}$, $u \in \mathbb{R}^K$ and $\odot$ is the Hadamard (matrix) product. Here, we have used the fact that $\mathbb{1}_{(p\neq q)} = \frac{1-pq}{2}$ for $p,q \in \{+1,-1\}$, implying:

$$-2X_kA_{kj}\mathbb{1}_{(X_k \neq X_j)} = A_{kj}[X_j - X_k], \tag{13}$$

hence recognizing a Laplacian term for the spin evolution in (11). By this computation, we can clearly identify the *homophily* term as well as the *selective exposure* term in (11).

A. Analysis of the NIMFA system

The deterministic system (11) is easier to analyze than the initial large-scale stochastic system: we are able to derive the entire set of equilibria and determine their stability.

Proposition 3. *Let* $g := \frac{\gamma}{\beta}$*. The set of attractive equilibria of the above dynamical system* (11) *is*

$$\mathcal{S} = \Big\{(x,a) : x = c\mathbb{1}, c \in [-1,1], a = v_*(c,g)\mathbb{K}\Big\}, \tag{14}$$

where $\mathbb{1}$ is the vector full of 1's: $\mathbb{1} = \sum_j e_j$ and

$$v_*(c,g) = \frac{1}{1+\frac{1-c^2}{2g}}. \tag{15}$$

Furthermore, there exists a set of unstable equilibria:

$$\mathcal{U} = \Big\{(x,a) : x_k = \pm 1 \ \forall k \text{ and } x_l = x_m \iff a_{lm} = 1 \text{ or } x_l \neq x_m \iff a_{lm} = 0\Big\}. \tag{16}$$

Proof. First suppose that the system has reached a consensus state: $x \in \{c\mathbb{1} : c \in [-1,1]\}$. We automatically have $\dot{x} = 0$. At consensus, the graph evolution yields

$$0 = \gamma(\mathbb{K} - A) - \frac{\beta(1-c^2)}{2}A = v_*(c,g)\mathbb{K} \tag{17}$$

with $v_*(c,g)$ given by (15). From this we can conclude that there is only one graph at consensual equilibrium $x_k = c \ \forall k$.

Let us now take in the more general case $\dot{A} = 0_{K\times K}$ and $\dot{x} = 0_K$. Suppose first $a_{ij} > 0 \ \forall i,j$, and define the homophily matrix as

$$H(x) := \frac{\mathbb{K} + xx^T}{2} \tag{18}$$

We then obtain

$$\begin{aligned} & \dot{a} = 0_{K\times K} \\ \iff & 0 = -a \odot \{\gamma H(x) + \beta(\mathbb{K} - H(x))\} + \gamma H(x) \\ \iff & a = f_\odot(H(x)), \end{aligned} \tag{19}$$

with

$$f(h) = \frac{\gamma h}{\gamma h + \beta(1-h)} \tag{20}$$

and $f_\odot : [0,1]^{K^2} \mapsto [0,1]^{K^2}$ the associated entry-wise map taking matrices as arguments. Note that f is monotonically strictly increasing, thus invertible. Therefore

$$\begin{aligned} f_\odot^{-1}(a) = H(x) &\implies \mathcal{L}(a) \circ f_\odot^{-1}(a) = 0 \\ &\implies \sum_j a_{lj}\Big[f^{-1}(a_{jm}) - f^{-1}(a_{lm})\Big] = 0 \ \forall l,m. \end{aligned} \tag{21}$$

Now, ad absurdum, suppose it exists a column m and two lines $l, L \in [K]$ such that $a_{lm} < a_{Lm}$. Because f^{-1} is also strictly increasing, $a_{Lj}[f^{-1}(a_{jm}) - f^{-1}(a_{Lm})] \leq 0$ $\forall j$, with at least one *strict* inequality for $j = l$. Thus, the equality 21 can not be verified for all l,m. This shows that $a_{lj} = c_j \ \forall l,j$, and then

$$\dot{x}_k = 0 \implies \sum_j c_j(x_j - x_k) = 0 \implies x = c\mathbb{1}, \ c \in [-1,1]. \tag{22}$$

And by the analysis made in the consensus state, it implies that the only possibility for the graph is $A = v_*(c,g)\mathbb{K}$, $c \in [-1,1]$.

Untill now, we have supposed that $a_{lm} > 0 \ \forall l,m$. Suppose now there exists at least one null coefficient: $a_{lm} = 0$. Then $\dot{a} = 0 \implies 1 + x_l x_m = 0 \iff x_l = x_m = \pm 1$. Without loss of generality, take $x_l = +1$ and $x_m = -1$. We have $a_{lj}(x_j - x_l) \leq 0$. This implies that either $x_j = x_l$, or $a_{lj} = 0$. Furthermore, in the case of $x_l = x_j = \pm 1$, we have necessarily $a_{lj} = 1$. The set $\mathcal{U}$ is thus well identified.

We now study the stability of all these equilibria. In order to show the attractiveness of $\mathcal{S}$, one can first notice that the phase space $[-1,1]^K \times [0,1]^{K^2}$ is compact. Then, every trajectory $\{(x(t), A(t)) : t \geq 0\}$ admits at least one accumulation point $(x^*, A^*) \in \mathcal{S} \bigcup \mathcal{U}$ for all initial datum $\big(x(0), A(0)\big) \in [-1,1]^K \times [0,1]^{K^2}$. Second, notice that there is a *diameter contraction*: $x_{min}(t) := \min_k x_k(t)$ is increasing, while $x_{max}(t) := \max_k x_k(t)$ is decreasing, provided it exists some $k \in [K]$ such that $\dot{x}(0) \neq 0$. Every accumulation is thus in $\mathcal{S}$: $\exists t_j \geq 0$, $||x(t_j) - c1_K|| < \epsilon$ and $||x(t) - c1_K|| < \epsilon$ for all $t \geq t_j$. This implies that for two distinct edges $e = lm$, $f = kj$,the edges dynamics are roughly the same. Rewrite indeed (11) as

$$\begin{aligned} \partial_t a_{lm} &= -\Big(\gamma h_{lm} + \beta(1 - h_{lm})\Big)a_{lm} + \gamma h_{lm} \\ &= u_{lm}(t)a_{lm} + h_{lm}(t) \end{aligned} \tag{23}$$

where $u_{lm}(t) < 0 \ \forall l,m,t$ and $h_{lm} = \frac{1+x_l x_m}{2}$. Each edge difference $(a_{lm} - a_{kj})$ evolves according to

$$\begin{aligned} \partial_t\left(a_{lm} - a_{kj}\right) &= u_{lm}(t)a_{lm} + h_{lm}(t) - (u_{kj}a_{kj} + h_{kj}) \\ &= u_{kj}\left(a_{lm} - a_{kj}\right) + \eta(t), \end{aligned} \tag{24}$$

where

$$\eta(t) = (v_{lm} - v_{kj}) + a_{lm}(u_{lm} - u_{kj}) \tag{25}$$

can be made arbitrarily small provided ϵ is chosen small enough. Recall $u_{lm} < -\min(\gamma,\beta)$. Whence

$$\partial_t(a_{lm} - a_{kj}) \leq -\min(\gamma,\beta)(a_{lm} - a_{kj}) + \eta_0. \tag{26}$$

By comparison principle (see for instance 3.4 of [26]), we have

$$(a_{lm} - a_{kj}) \leq \min(\gamma,\beta) \text{ for } t \text{ large enough.} \tag{27}$$

This allows us to conclude that $A(t)$ converges to the set $\{vA : v \in [0,1]\}$. The previous derivation provides a closed-form analytical expression of the value v_* as a function of the consensus value c reached by the spin profile. ∎

Remark 4. *The set of stable equilibria $\mathcal{S}$ is made up of a continuum of points independent of ϕ, while the unstable ones are just isolated points in the compact*

phase space $\Psi := [-1,+1]^K \times [0,1]^{K^2}$. *The points in the set* $\mathcal{U}$ *corresponds to the absorbing configurations of the initial stochastic system, where the system is maximally polarised and the discordance is zero.*

The NIMFA method also gives as output a closed-form expression of the discordance. Let first extend the definition of the discordance to continuous systems as

$$\mathcal{D}(x,a) := \frac{1}{K^2}\sum_{lm} a_{lm}\frac{1-x_l x_m}{2}. \tag{28}$$

Corollary 5. *Consider the system having reached the surface of equilibria computed in proposition 3:* $(x,a) \in \mathcal{S}$ *which implies* $x = c\mathbb{1}$ *for some* $c \in [-1,+1]$ *and* $a = v_*(c,g)\mathbb{K}$. *Then discordance reads as*

$$\mathcal{D}(x,a) = v_*(c,g)\frac{1-c^2}{2}, \tag{29}$$

where v_* *is defined in proposition 3.*

Proof. Because by definition

$$\mathcal{D} = \frac{1}{K^2}\sum_{lm} a_{lm}\mathbb{1}_{(x_l \neq x_m)} = \frac{1}{2K^2}\sum_{lm} a_{lm}(1-x_l x_m) \tag{30}$$

the result is straightforward in view of proposition 3. ■

B. Numerical simulations

In order to represent visually the dynamics, the Markov process is reduced to three global estimators, namely

$$\begin{array}{l} \overline{X} := \frac{1}{K}\sum_j X_j \\ \overline{A} := \frac{1}{K^2}\sum_{lm} A_{lm} \text{ and} \\ D := \frac{1}{K^2}\sum_{lm} A_{lm}\mathbb{1}_{(X_l \neq X_m)} \end{array} \tag{31}$$

$\overline{X}$ is the mean spin profile, $\overline{A}$ is the global density of links and D is the discordance. In Figure 2 , five trajectories are represented in the $\overline{X}-\overline{A}$ axis, with slightly different initial configurations. We can see that all the trajectories are quasi-attracted by the consensual equilibria line analytically computed in proposition 3, although a small but consistent gap subsists. In the second plot, three trajectories are represented in the $\overline{X}-D$ axis. Also, in that case, the theoretical NIMFA-based discordance seems similar yet quantitatively distinct.

In order to understand this bias, let us represent the asymptotic system $K \longrightarrow +\infty$ with a continuum of population $u \in [0,1]$, and the associated spin profile and generalized matrix $\{X_u, A_{uv} : u,v \in [0,1]\}$. The NIMFA actually partitions in an arbitrary fashion the population in K cells and applies a cell-wise averaging:

$$x_j \sim \frac{1}{K}\int_{u\in I_j} X_u du \quad a_{lm} \sim \frac{1}{K^2}\int_{(u,v)\in I_l\times I_m} A_{uv}dudv \tag{32}$$

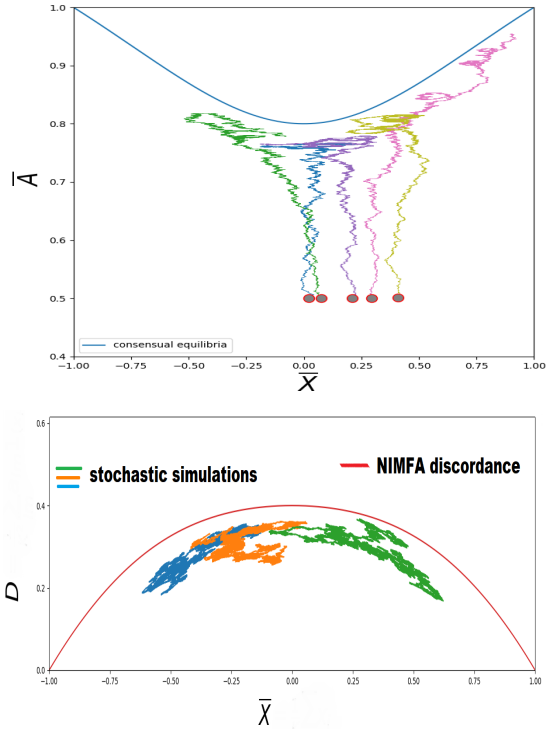

FIG. 2. Simulations have been performed in the metastable regime: $(\phi,\beta,\gamma) = (4,1,4)$, and $K = 800$. The grey points are the initial configurations. *We see that the system is attracted by the blue curve analytically computed in proposition 3, although there is still a small gap between the simulations and the theoretical result. A similar observation can be stated for the figure below: we see that the three independent stochastic simulations have roughly the same shape as the theoretical NIMFA discordance line (in red), but here also a substantial gap persists.*

for $j \in [K]$, with $I_j = [\frac{j}{K}, \frac{j+1}{K}[$. Thus, this approximation puts in the same category discordant links $\{(lm) : x_l \neq x_m\}$ and concordant links $\{(lm) : x_l = x_m\}$, leading to a dead-weight loss of information. To see this, let us take the following example: suppose $x_l = x_m = 0$ and $a_{lm} = \frac{1}{2}$. This means that half of the mass of cell l has a positive spin and the other half has a negative spin, and the same with cell m. Nonetheless, one can not in any way determine whether the links from cell l to cell m are discordant or concordant, and in which proportion. Thus, as depicted in Figure 3, one of the drawbacks of the NIMFA is the ambiguity. It can correspond either to a case of discordance free: all agents of cell l are linked toward people in m of the same spin and *only* with them, or it can correspond to maximum discordance (and zero concordance) configuration. In the next section, an alternative system of coordinates is presented to make the distinction between concordant edges and discordant edges, and then assign distinct dynamics to these possible cases.

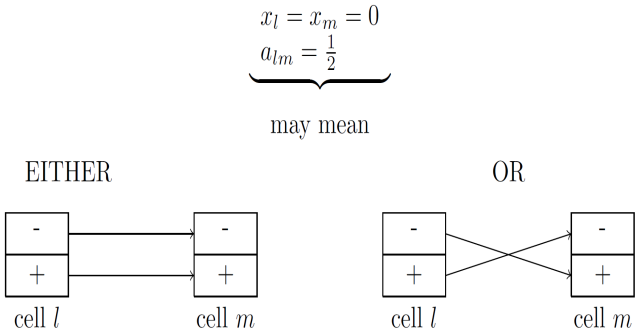

FIG. 3. In each cell l, m, a first half of the population is $+1$ and the other half is -1.

IV. NEW BLOCKWISE COORDINATE SYSTEM

Instead of considering the spin profile, let us just keep the graph structure. We separate the links in four categories $\mathcal{C}^1, \mathcal{D}^1, \mathcal{C}^0, \mathcal{D}^0 \in \{0,1\}^{K^2}$ according to two criteria: *concordant* ($\mathcal{C}$) or *discordant* ($\mathcal{D}$), and *present* (indexed with a one), or *absent* (indexed with a zero). This partition leads to the following equivalences:

$$\begin{array}{rcl} a_{lm} = 1 \wedge x_l = x_m & \iff & \mathcal{C}^1_{lm} = 1 \\ a_{lm} = 0 \wedge x_l = x_m & \iff & \mathcal{C}^0_{lm} = 1 \\ a_{lm} = 1 \wedge x_l \neq x_m & \iff & \mathcal{D}^1_{lm} = 1 \\ a_{lm} = 0 \wedge x_l \neq x_m & \iff & \mathcal{D}^0_{lm} = 1 \end{array} \tag{33}$$

In this new coordinate system, the stochastic evolution equation is rewritten as:

$$\begin{cases} d\mathcal{C}^1 &= +\mathcal{C}^0 \odot \mathcal{N}^\gamma(dt) + (\mathcal{D}^1 - \mathcal{C}^1) \odot F(dt), \\ d\mathcal{C}^0 &= -\mathcal{C}^0 \odot \mathcal{N}^\gamma(dt) + (\mathcal{D}^0 - \mathcal{C}^0) \odot F(dt), \\ d\mathcal{D}^1 &= -\mathcal{D}^1 \odot \mathcal{N}^\beta(dt) + (\mathcal{C}^1 - \mathcal{D}^1) \odot F(dt), \\ d\mathcal{D}^0 &= +\mathcal{D}^1 \odot \mathcal{N}^\beta(dt) + (\mathcal{C}^0 - \mathcal{D}^0) \odot F(dt), \end{cases} \tag{34}$$

where

$$F(dt) := \left(\mathcal{D}^1 \odot \mathcal{N}^{\frac{\phi}{K}}(dt)\right) \circ \mathbb{K} + \mathbb{K} \circ \left(\mathcal{D}^1 \odot \mathcal{N}^{\frac{\phi}{K}}(dt)\right)^\top \tag{35}$$

Here $\mathcal{N}^\alpha(t) = \left(\mathcal{N}^\alpha_{lm}(t)\right)_{(l,m)\in[K]^2}$ is a square matrix of dimension K stacking all the independent Poisson processes of intensity $\alpha > 0$, $\alpha \in \{\frac{\phi}{K}, \beta, \gamma\}$. One can see that the first terms of the right-hand side correspond to the *network dynamics*, while the second terms correspond to the flip dynamics with the $\mathcal{N}^{\frac{\phi}{K}}$ as driving processes. Figure 4 provides a schematic picture of the different flows between the four compartments defined above.

A. Dimensionality reduction

System (34) describes the initial one (5) but from another viewpoint. Its main advantage is that it separates conveniently the discordant and concordant edges, and

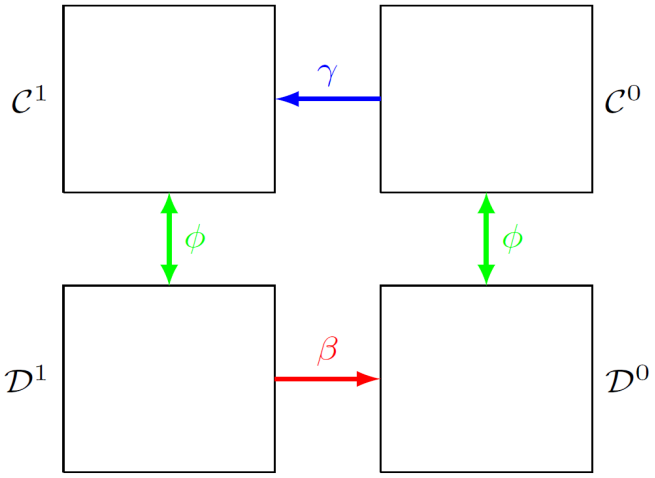

FIG. 4. A partition of the edges linked with flows.

these two categories of edges display very different behavior. It has to be noticed that through these coordinates, one has no access to the mean spin profile $\overline{X}$ neither the proportion of agents with positive spin

$$m := \frac{1}{K} \sum_j \mathbb{1}_{(X_j = 1)}. \tag{36}$$

Because of its high dimensionality, actually $4K^2$, it seems intractable. Proposition 3 suggests to circumvent this difficulty by making the following *homogeneity hypothesis*:

$$\mathcal{C}^\sigma \approx c_\sigma \mathbb{K} \text{ and } \mathcal{D}^\sigma \approx d_\sigma \mathbb{K}, \tag{37}$$

for some $d_\sigma, c_\sigma \in [0,1], \sigma \in \{1,0\}$ with vanishing randomness when K gets large. Some details of this assumption will be given in the next section. The large-scale stochastic system (34) can then be described by a nonlinear 4-dimensional deterministic ODE:

$$\partial_t Y_t = \Psi(Y_t) = N_{\beta,\gamma} Y_t + 2\phi d_1 M Y_t \tag{38}$$

where

$$Y = \begin{bmatrix} c_1 \\ c_0 \\ d_1 \\ d_0 \end{bmatrix}, N_{\beta,\gamma} := \begin{bmatrix} 0 & \gamma & 0 & 0 \\ 0 & -\gamma & 0 & 0 \\ 0 & 0 & -\beta & 0 \\ 0 & 0 & \beta & 0 \end{bmatrix} \tag{39}$$

and

$$M := \begin{bmatrix} -1 & 0 & +1 & 0 \\ 0 & -1 & 0 & +1 \\ +1 & 0 & -1 & 0 \\ 0 & +1 & 0 & -1 \end{bmatrix}. \tag{40}$$

Remark 6. *Contrary to system* (11) *where the absorbing points are always unstable and repulsive regardless of the models' parameters, this system displays a stable discordance-free region for* $\phi \ll \beta$*:*

Let us consider the discordance-free absorbing points that are easily identifiable:

$$\mathcal{A} = \left\{ \begin{bmatrix} u & 0 & 0 & 1-u \end{bmatrix}^T : \; u \in [\frac{1}{2}, 1] \right\} \tag{41}$$

Setting $u = 1$ corresponds to a global consensus, while if $u = \frac{1}{2}$, then the two blocks are of same size. By linearization of the vector field Ψ in (38), we get for $y \in \mathcal{A}$

$$\partial\Psi_y = \begin{bmatrix} 0 & \gamma & -2\phi u & 0 \\ 0 & -\gamma & 2\phi(1-u) & 0 \\ 0 & 0 & -\beta + 2\phi u & 0 \\ 0 & 0 & \beta + 2\phi(u-1) & 0 \end{bmatrix} \tag{42}$$

A simple examination of the eigenvalues leads to

$$Sp\ \partial\Psi_y = \{0, 0, -\gamma, 2\phi u - \beta\}. \tag{43}$$

Furthermore, the null eigenvalue is semisimple. Then, by linearization method (thm. 3.15 of [27]), for β high enough, that is $\phi < \frac{\beta}{2u}$, the point y is stable.

Furthermore, system (38) being low dimensional, we can now give an explicit formula for the equilibria.

Proposition 7 (characterization of the equilibria)**.** *For any values ϕ, β, γ, in the coordinates (c_1, d_1, m), the surface of equilibria $\mathcal{S}_{eq}$ of the reduced system (38) is given by*

$$\mathcal{S}_{eq} = \Big\{ (c_1, d_1, m) : d_1 = g\big(1 - c_1 - 2m(1-m)\big) \Big\}. \tag{44}$$

Proof. Recall $g := \frac{\gamma}{\beta}$. At equilibrium: $\partial_t Y = 0$, we have

$$d_1 = g c_0, \tag{45}$$

and by construction, $d_1 + c_1 + d_0 + c_0 = 1$ and $2m(1-m) = d_0 + d_1$ at all times. Combining the last three identities yields the last proposition. ■

B. Computation of the discordance

We are now able to derive a formula for the global discordance d_1 at equilibrium: the third line of (38) yields

$$0 = -\beta d_1 + (c_1 - d_1) 2\phi d_1. \tag{46}$$

Then, adding the first and the second lines gives $0 = (d_1 - c_1 + d_0 - c_0)\, 2\phi d_1$. Because $d_1 > 0$, we thus get:

$$d_1 + d_0 = c_1 + c_0 = \frac{1}{2}. \tag{47}$$

Recall $d_1 = g c_0$, combining all the last identities allows us to state the following proposition.

Proposition 8. *(limit value for the discordance) For high K, the discordance d_1 of system (X, A) converges toward the value $d^* = \frac{1}{2} \times \frac{1 - \frac{\beta}{\phi}}{1 + \frac{\beta}{\gamma}} \in [0, \frac{1}{2}]$.*

Remark 9. *This quantity does make sense only for $\phi > \beta$. More specifically, for $\phi \gg \beta$ and $\gamma \gg \beta$, d^* is almost maximal, namely $d^* \approx \frac{1}{2}$. On the contrary, for $\beta < \phi$, the system is attracted toward the discordance-free region.*

C. Numerical plots

Figure 5 shows how close is the actual process to the analytical surface $\mathcal{S}_{eq}$ when projected to the phase space (c_1, m, d_1). Figure 6 displays four independent numerical simulations in the metastable regime with the same model's parameters. The horizontal line d^* corresponds to the value obtained in proposition 8. When taking smaller ϕ, we observe that discordance is vanishing: see Figure 7.

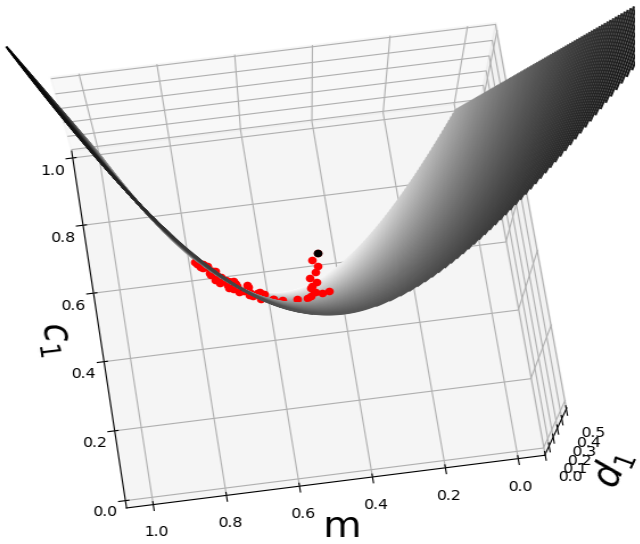

FIG. 5. $\mathcal{S}_{eq}$ is represented by the grey surface. Red points are sample of the overall trajectory starting at the black point, under the metastable regime: $(\phi, \beta, \gamma) = (4, 1, 4)$, and $K = 800$. *We see that there is no gap between the surface of theoretical surface and the stochastic simulation.*

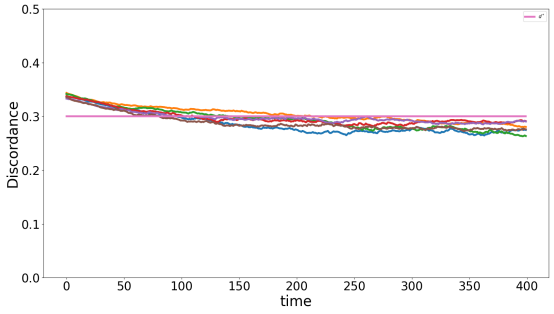

FIG. 6. $(\phi, \beta, \gamma) = (4, 1, 4)$, $K = 800$. Here is a plot of six independent simulations for the discordance d_1. *We see that in the metastable regime, discordance maintains and is close to the value computed via block-coordinates (represented as an horizontal pink line on the plot), that is $d^* = 0.3$.*

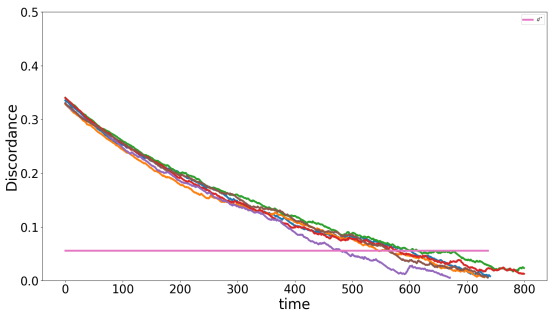

FIG. 7. $(\phi, \beta, \gamma) = (1, 0.8, 1)$, and $K = 800$. Six independent plots have been performed. *We see that there is a fast extinction of discordance when $\beta \approx \phi$ (subcritical regime).*

V. DISCUSSION

The results of the preceding section rely on the *homogeneity assumption* obtained by the standard NIMFA method (see proposition 3). Because the spins and the edges are binary $X_k \in \{+1, -1\}^K$ and $A_{lm}, \mathcal{C}^\sigma_{lm}, \mathcal{D}^\sigma_{lm} \in \{0, 1\}$, it is necessary to clarify that $\mathcal{C}^\sigma$ is *roughly equal to* some $c\mathbb{K}$ for $c \in [0, 1]$. Actually, this approximation has to be taken in the *macroscopic viewpoint*, that is when taking an arbitrary but infinite subset of agents $\{j \in [K] : \frac{j}{K} \in U\}$ for some interval $U \subset [0, 1]$. Sampling this way and taking the associated averages $\overline{X}_U, \overline{A}_{UV}$ defined below, we then obtain, when K tends to $+\infty$, deterministic limits with identical trajectories, regardless of the choice of $U, V \subset [0, 1]$. It is what we call *homogeneity*.

Conjecture 10. *Recall that $|U|$ stands for the Lebesgue measure of an interval U in $\mathbb{R}$. Define the partial average:*

$$\overline{X}^K_U := \frac{1}{K|U|} \sum_j X_j \mathbb{1}_U(\frac{j}{K}) \tag{48}$$

for any interval $U \subset [0, 1]$ with $U = [a, b], a < b$. Then, $\overline{X}^K_U$ converges towards a deterministic and continuous trajectory as $K \longrightarrow +\infty$, under the hypothesis that the initial samples $(X_k(0))_{k\in[K]}$ and $(A_{lm})_{l,m}$ are i.i.d. This statement is also valid for the functionals

$$\overline{A}^K_{UV} := \frac{1}{K^2|U||V|} \sum_{lm} A_{lm} \mathbb{1}_{U\times V} \left(\frac{l}{K}, \frac{m}{K}\right) \tag{49}$$

Especially, the global density of links defined as

$$\overline{A}^K = \frac{1}{K^2} \sum_{lm} a_{lm} \tag{50}$$

converges toward a deterministic and continuous trajectory. Furthermore, the limiting trajectories are identical: For any $U, V, U', V' \subset [0, 1]$,

$$||\overline{X}^K_U - \overline{X}^K_{U'}||_{\infty,T} \longrightarrow 0 \text{ and} \tag{51}$$

$$||\overline{A}^K_{UV} - \overline{A}^K_{U'V'}||_{\infty,T} \longrightarrow 0 \tag{52}$$

as $K \longrightarrow +\infty$, provided that the entrance sample is i.i.d: $a_{lm}(0) = 1$ with probability a_0 for all l, m, $X_k = +1$ with probability x_0 all variables being independent, and where $||.||_{\infty,T}$ is the uniform norm over the set of bounded real-valued functions defined on the time interval $[0, T]$: $||u|| := \sup_{s\in[0,T]} |u(s)|$.

Remark 11. *The hypothesis on the entrance law is crucial. Indeed, suppose that we set $X_k(0) = +1$ with probability 1 for $k < \frac{K}{2}$ and $X_k(0) = -1$ with probability 1 for $k \geq \frac{K}{2}$, which is not an i.i.d entrance law. Setting $\beta \gg \phi$ would yield $\overline{X}_{[0,\frac{1}{2}]} \approx +1$ and $\overline{X}_{[\frac{1}{2},1]} \approx -1$, which would contradict the last result.*

Remark 12. *The type of convergence stated above via partial sampling along intervals $U \in [0, 1]$ has strong links with the cut metric over dense graphs. Roughly speaking, it says that the sequence of random trajectories $(A^K(t))_t$ admits a correctly defined limit object W_t [28].*

In order to verify numerically that the graph displays an homogeneous behaviour, we have partitioned the population in 4 equal parts $I_j := \{k \in [K] : k \equiv j \bmod 4\}$. We thus obtain a partition $\mathcal{P}_4$ of size 4. Then, for $U, V \in \mathcal{P}_4 := (I_j)_{1\leq j\leq 4}$, we compute the average blockwise defined as:

$$\overline{A}_{UV} = (\frac{K}{4})^{-2} \sum_{lm} A_{lm} \mathbb{1}_{U\times V}(l, m) \tag{53}$$

We then obtain 16 trajectories. We have performed the simulations for several values of K (see Figure 8). For increasing K, it is clear that the 16 curves concentrate over the same trajectory and randomness decays. We also display the partial means for the spins: $\overline{X}_U, U \in (I_j)_j$. We observe that the edges means $\overline{A}_{lm}$ converge much faster compared to the spins' ones $\overline{X}_U$ because each average $\overline{A}_{UV}$ contains $(\frac{K}{4})^2 = \frac{K^2}{16}$ terms whereas the spin averages *only* contains $\frac{K}{4}$ terms.

VI. CONCLUSION AND FUTURE WORK

In this paper, we have presented a new continuous-time AVM where node and edge steps are not simultaneous. By taking into account additional permissible configurations, the model is more flexible and satisfactory. Its analysis by the standard NIMFA was refined by a precise change of coordinates using a blockwise approach. Moreover, in the case of dense graphs, a phenomenon that we called *homogeneity* has been conjectured when K becomes large. Although we could not give a rigorous proof, numerous numerical simulations were provided to corroborate our intuition. This may be an interesting topic for further investigation.

ACKNOWLEDGMENTS

This work was supported by the Agence Nationale de la Recherche (ANR) through the project NICETWEET

(ANR-20-CE48-0009).

[1] T. M. Liggett and T. M. Liggett, *Interacting particle systems*, Vol. 2 (Springer, 1985).

[2] C. Castellano, M. A. Muñoz, and R. Pastor-Satorras, Nonlinear q-voter model, Physical Review E **80**, 041129 (2009).

[3] E. Yildiz, A. Ozdaglar, D. Acemoglu, A. Saberi, and A. Scaglione, Binary opinion dynamics with stubborn agents, ACM Transactions on Economics and Computation (TEAC) **1**, 1 (2013).

[4] N. Masuda, Voter models with contrarian agents, Physical Review E **88**, 052803 (2013).

[5] A. Carro, R. Toral, and M. San Miguel, The noisy voter model on complex networks, Scientific reports **6**, 1 (2016).

[6] Y. Dong, M. Zhan, G. Kou, Z. Ding, and H. Liang, A survey on the fusion process in opinion dynamics, Information Fusion **43**, 57 (2018).

[7] M. McPherson, L. Smith-Lovin, and J. M. Cook, Birds of a feather: Homophily in social networks, Annual review of sociology , 415 (2001).

[8] D. Zillmann and J. Bryant, *Selective exposure to communication* (Routledge, 2013).

[9] T. Gross and B. Blasius, Adaptive coevolutionary networks: a review, Journal of the Royal Society Interface **5**, 259 (2008).

[10] S. Trajanovski, D. Guo, and P. Van Mieghem, From epidemics to information propagation: Striking differences in structurally similar adaptive network models, Physical Review E **92**, 030801 (2015).

[11] T. Raducha, B. Min, and M. San Miguel, Coevolving nonlinear voter model with triadic closure, EPL (Europhysics Letters) **124**, 30001 (2018).

[12] N. Malik, F. Shi, H.-W. Lee, and P. J. Mucha, Transitivity reinforcement in the coevolving voter model, Chaos: An Interdisciplinary Journal of Nonlinear Science **26**, 123112 (2016).

[13] T. Rogers and T. Gross, Consensus time and conformity in the adaptive voter model, Physical Review E **88**, 030102 (2013).

[14] P. Holme and M. E. Newman, Nonequilibrium phase transition in the coevolution of networks and opinions, Physical Review E **74**, 056108 (2006).

[15] G. Zschaler, G. A. Böhme, M. Seißinger, C. Huepe, and T. Gross, Early fragmentation in the adaptive voter model on directed networks, Physical Review E **85**, 046107 (2012).

[16] R. Basu and A. Sly, Evolving voter model on dense random graphs, The Annals of Applied Probability **27**, 1235 (2017).

[17] T. M. Liggett *et al.*, *Stochastic interacting systems: contact, voter and exclusion processes*, Vol. 324 (springer science & Business Media, 1999).

[18] V. Sood and S. Redner, Voter model on heterogeneous graphs, Physical review letters **94**, 178701 (2005).

[19] M. E. Yildiz, R. Pagliari, A. Ozdaglar, and A. Scaglione, Voting models in random networks, in *2010 information theory and applications workshop (ITA)* (IEEE, 2010) pp. 1–7.

[20] N. J. Stroud, Polarization and partisan selective exposure, Journal of communication **60**, 556 (2010).

[21] F. Zuiderveen Borgesius, D. Trilling, J. Möller, B. Bodó, C. H. De Vreese, and N. Helberger, Should we worry about filter bubbles?, Internet Policy Review. Journal on Internet Regulation **5** (2016).

[22] D. Spohr, Fake news and ideological polarization: Filter bubbles and selective exposure on social media, Business information review **34**, 150 (2017).

[23] D. DiFranzo and K. Gloria-Garcia, Filter bubbles and fake news, XRDS: Crossroads, The ACM Magazine for Students **23**, 32 (2017).

[24] E. Jacob, A. Linker, and P. Mörters, Metastability of the contact process on fast evolving scale-free networks, The Annals of Applied Probability **29**, 2654 (2019).

[25] P. Van Mieghem, The n-intertwined sis epidemic network model, Computing **93**, 147 (2011).

[26] H. Khalil, Nonlinear systems, printice-hall, Upper Saddle River, NJ **3** (1996).

[27] W. M. Haddad and V. Chellaboina, Nonlinear dynamical systems and control, in *Nonlinear Dynamical Systems and Control* (Princeton university press, 2011).

[28] C. Borgs, J. T. Chayes, L. Lovász, V. T. Sós, and K. Vesztergombi, Convergent sequences of dense graphs i: Subgraph frequencies, metric properties and testing, Advances in Mathematics **219**, 1801 (2008).

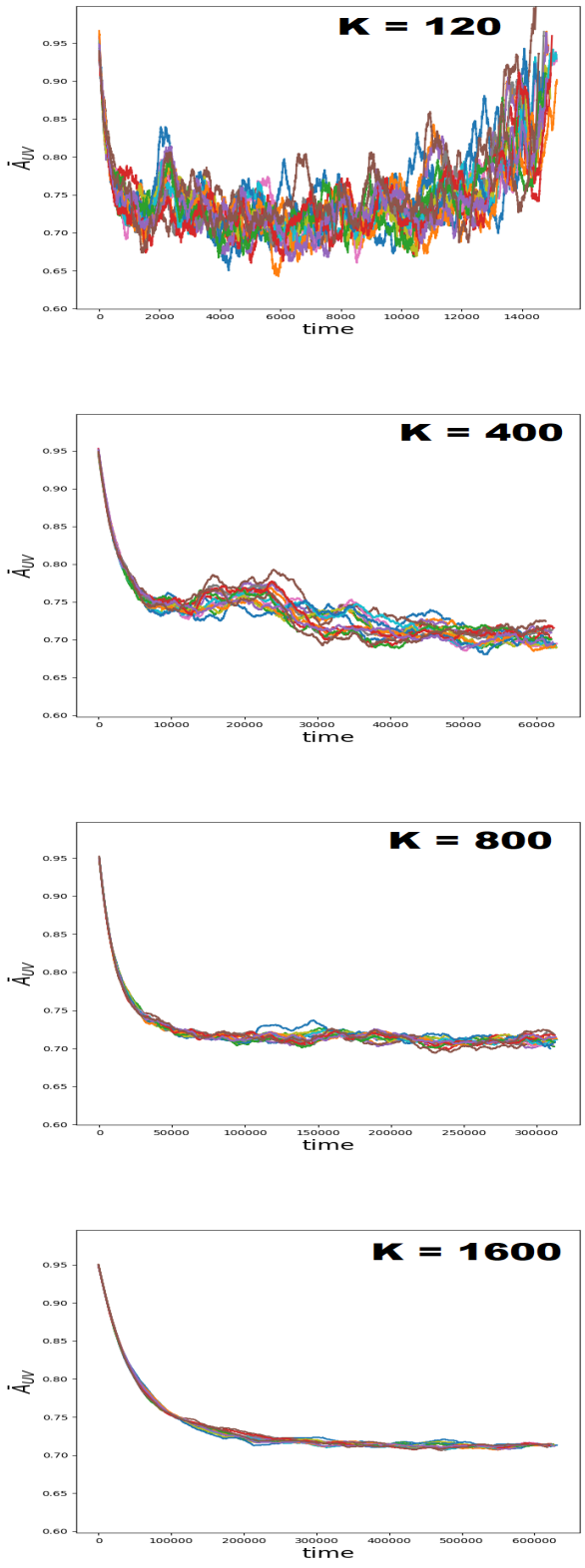

FIG. 8. For several values of K, we plot the curves of the 16 partial edges means $\{t \mapsto \overline{A}_{UV}(t) : U, V \in \mathcal{P}_4\}$. In all cases, models' parameters are taken constant: $(\phi, \beta, \gamma) = (4, 1, 4)$. At initial times, all random variables are taken i.i.d: $a_{lm}(0) = 1$ with probability 0,95. *The concentration of the all trajectories around the same curve when K grows is visible when comparing $K = 120$ and $K = 1600$.*

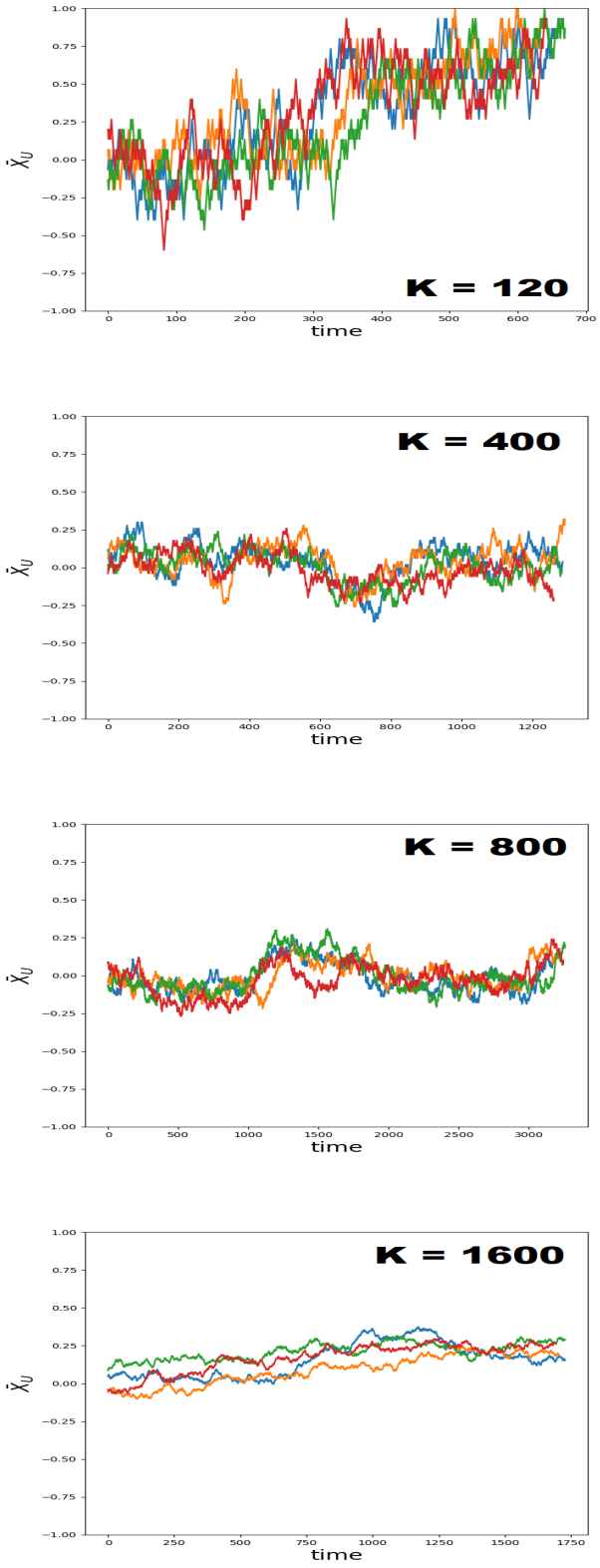

FIG. 9. For several values of K, we plot the curves of the four partial edges means $\{t \mapsto \overline{X}_U(t) : U \in \mathcal{P}_4\}$, with $(\phi, \beta, \gamma) = (4, 1, 4)$. For all simulations $x_k(0)$ are taken i.i.d with $x_k(0) = +1$ with probability $\frac{1}{2}$. *Here too, a concentration effect occurs, but it is less pronounced because the spin profile includes less variables as the graph.*